

# Search for Low-Mass WIMPs with SuperCDMS

R. Agnese,<sup>18</sup> A.J. Anderson,<sup>4,\*</sup> M. Asai,<sup>8</sup> D. Balakishiyeva,<sup>18</sup> R. Basu Thakur,<sup>2,19</sup> D.A. Bauer,<sup>2</sup> J. Beaty,<sup>20</sup> J. Billard,<sup>4</sup> A. Borgland,<sup>8</sup> M.A. Bowles,<sup>11</sup> D. Brandt,<sup>8</sup> P.L. Brink,<sup>8</sup> R. Bunker,<sup>11</sup> B. Cabrera,<sup>10</sup> D.O. Caldwell,<sup>15</sup> D.G. Cerdeno,<sup>13</sup> H. Chagani,<sup>20</sup> Y. Chen,<sup>11</sup> M. Cherry,<sup>8</sup> J. Cooley,<sup>9</sup> B. Cornell,<sup>1</sup> C.H. Crewdson,<sup>21</sup> P. Cushman,<sup>20</sup> M. Daal,<sup>14</sup> D. DeVaney,<sup>20</sup> P.C.F. Di Stefano,<sup>21</sup> E. Do Couto E Silva,<sup>8</sup> T. Doughty,<sup>14</sup> L. Esteban,<sup>13</sup> S. Fallows,<sup>20</sup> E. Figueroa-Feliciano,<sup>4</sup> G.L. Godfrey,<sup>8</sup> S.R. Golwala,<sup>1</sup> J. Hall,<sup>5</sup> S. Hansen,<sup>2</sup> H.R. Harris,<sup>12</sup> S.A. Hertel,<sup>4</sup> B.A. Hines,<sup>16</sup> T. Hofer,<sup>20</sup> D. Holmgren,<sup>2</sup> L. Hsu,<sup>2</sup> M.E. Huber,<sup>16</sup> A. Jastram,<sup>12</sup> O. Kamaev,<sup>21</sup> B. Kara,<sup>9</sup> M.H. Kelsey,<sup>8</sup> S. Kenany,<sup>14</sup> A. Kennedy,<sup>20</sup> M. Kiveni,<sup>11</sup> K. Koch,<sup>20</sup> A. Leder,<sup>4</sup> B. Loer,<sup>2</sup> E. Lopez Asamar,<sup>13</sup> R. Mahapatra,<sup>12</sup> V. Mandic,<sup>20</sup> C. Martinez,<sup>21</sup> K.A. McCarthy,<sup>4</sup> N. Mirabolfathi,<sup>14</sup> R.A. Moffatt,<sup>10</sup> R.H. Nelson,<sup>1</sup> L. Novak,<sup>10</sup> K. Page,<sup>21</sup> R. Partridge,<sup>8</sup> M. Pepin,<sup>20</sup> A. Phipps,<sup>14</sup> M. Platt,<sup>12</sup> K. Prasad,<sup>12</sup> M. Pyle,<sup>14</sup> H. Qiu,<sup>9</sup> W. Rau,<sup>21</sup> P. Redl,<sup>10</sup> A. Reisetter,<sup>17</sup> R.W. Resch,<sup>8</sup> Y. Ricci,<sup>21</sup> M. Ruschman,<sup>2</sup> T. Saab,<sup>18</sup> B. Sadoulet,<sup>14,3</sup> J. Sander,<sup>22</sup> R.L. Schmitt,<sup>2</sup> K. Schneck,<sup>8</sup> R.W. Schnee,<sup>11</sup> S. Scorza,<sup>9</sup> D.N. Seitz,<sup>14</sup> B. Serfass,<sup>14</sup> B. Shank,<sup>10</sup> D. Speller,<sup>14</sup> A. Tomada,<sup>8</sup> S. Upadhyayula,<sup>12</sup> A.N. Villano,<sup>20</sup> B. Welliver,<sup>18</sup> D.H. Wright,<sup>8</sup> S. Yellin,<sup>10</sup> J.J. Yen,<sup>10</sup> B.A. Young,<sup>7</sup> and J. Zhang<sup>20</sup>

(The SuperCDMS Collaboration)

<sup>1</sup>*Division of Physics, Mathematics, & Astronomy,*

*California Institute of Technology, Pasadena, CA 91125, USA*

<sup>2</sup>*Fermi National Accelerator Laboratory, Batavia, IL 60510, USA*

<sup>3</sup>*Lawrence Berkeley National Laboratory, Berkeley, CA 94720, USA*

<sup>4</sup>*Department of Physics, Massachusetts Institute of Technology, Cambridge, MA 02139, USA*

<sup>5</sup>*Pacific Northwest National Laboratory, Richland, WA 99352, USA*

<sup>6</sup>*Department of Physics, Queen's University, Kingston, ON K7L 3N6, Canada*

<sup>7</sup>*Department of Physics, Santa Clara University, Santa Clara, CA 95053, USA*

<sup>8</sup>*SLAC National Accelerator Laboratory/Kavli Institute for Particle*

*Astrophysics and Cosmology, 2575 Sand Hill Road, Menlo Park 94025, CA*

<sup>9</sup>*Department of Physics, Southern Methodist University, Dallas, TX 75275, USA*

<sup>10</sup>*Department of Physics, Stanford University, Stanford, CA 94305, USA*

<sup>11</sup>*Department of Physics, Syracuse University, Syracuse, NY 13244, USA*

<sup>12</sup>*Department of Physics, Texas A&M University, College Station, TX 77843, USA*

<sup>13</sup>*Departamento de Física Teórica and Instituto de Física Teórica UAM/CSIC, Universidad Autónoma de Madrid, 28049 Madrid, Spain*

<sup>14</sup>*Department of Physics, University of California, Berkeley, CA 94720, USA*

<sup>15</sup>*Department of Physics, University of California, Santa Barbara, CA 93106, USA*

<sup>16</sup>*Department of Physics, University of Colorado Denver, Denver, CO 80217, USA*

<sup>17</sup>*Department of Physics, University of Evansville, Evansville, IN 47722, USA*

<sup>18</sup>*Department of Physics, University of Florida, Gainesville, FL 32611, USA*

<sup>19</sup>*Department of Physics, University of Illinois at Urbana-Champaign, Urbana, IL 61801, USA*

<sup>20</sup>*School of Physics & Astronomy, University of Minnesota, Minneapolis, MN 55455, USA*

<sup>21</sup>*Department of Physics, Queen's University, Kingston ON, Canada K7L 3N6*

<sup>22</sup>*Department of Physics, University of South Dakota, Vermillion, SD 57069, USA*

We report a first search for weakly interacting massive particles (WIMPs) using the background rejection capabilities of SuperCDMS. An exposure of 577 kg-days was analyzed for WIMPs with mass  $< 30 \text{ GeV}/c^2$ , with the signal region blinded. Eleven events were observed after unblinding. We set an upper limit on the spin-independent WIMP-nucleon cross section of  $1.2 \times 10^{-42} \text{ cm}^2$  at  $8 \text{ GeV}/c^2$ . This result is in tension with WIMP interpretations of recent experiments and probes new parameter space for WIMP-nucleon scattering for WIMP masses  $< 6 \text{ GeV}/c^2$ .

Evidence on galactic and cosmological scales strongly indicates that  $\sim 80\%$  of the matter density of the Universe consists of non-luminous, non-baryonic dark matter, whose particle nature remains unknown [1]. Weakly interacting massive particles (WIMPs) are one class of theoretically well-motivated candidates for dark matter and may be detectable by searching for keV-scale nuclear recoils in terrestrial detectors [2]. Recent excesses of events reported by CDMS II (Si) [3], CoGeNT [4],

CRESST-II [5], DAMA [6], and possible indirect evidence from gamma rays from the galactic center [7], may be interpreted as a light WIMP with mass in the 6–30  $\text{GeV}/c^2$  range. A variety of theoretical models also favor light WIMPs in this mass range [8–15].

Since light WIMPs produce only low-energy nuclear recoils, experiments optimized for masses  $\gtrsim 30 \text{ GeV}/c^2$  have searched for light WIMPs by lowering their analysis energy threshold [16–19]. This additional sensitiv-

ity comes with higher background rates because resolution effects degrade particle discrimination at low energies. Following this approach, we analyzed low-energy recoils in the range 1.6–10 keV<sub>nr</sub> (nuclear-recoil equivalent energy) from the SuperCDMS experiment at the Soudan Underground Laboratory (SUL) [20]. Although background discrimination gradually degrades with decreasing event energy, some discrimination can still be achieved using the relative signal measured by the different readout channels on each detector.

SuperCDMS at Soudan is an upgrade to the Cryogenic Dark Matter Search (CDMS II) [21] with new detector hardware, and is operating in the same location with the same low-radioactivity setup [22]. The target consists of fifteen 0.6-kg cylindrical germanium crystals stacked in groups of three to form five towers. Each crystal is instrumented with interleaved ionization and phonon sensors on its flat faces (iZIP). iZIPs measure ionization and phonon energy, from which we derive the recoil energy and the “ionization yield,” the ratio between ionization and recoil energy. Electron-recoil backgrounds are distinguished from nuclear recoils by the fact that nuclear recoils exhibit a reduced ionization yield compared to electron recoils. Nuclear recoils are expected from WIMPs, and electron recoils from most backgrounds. The iZIP sensor layout improves the ability to define a fiducial volume in the bulk (fiducialization) over the CDMS II design [23]. The partitioning (i.e. asymmetry) of phonon or ionization energy between guard and inner sensors provides radial fiducialization, and partitioning between sensors on the two faces provides  $z$  fiducialization. Such fiducialization rejects events in the peripheral regions of the detectors. These “surface events” often suffer from reduced ionization signal, thus polluting the WIMP signal region.

The SuperCDMS payload has been operating in SUL since March 2012. The data presented here, recorded between October 2012 and June 2013, are a subset of the ongoing exposure. The seven detectors with the lowest trigger thresholds are used for this search. The remaining detectors were used to reject events with energy deposition in more than one detector. Consistency tests are used to remove periods of abnormal detector behavior and elevated noise. After accounting for these losses, the exposure is 577 kg-days. To prevent bias when defining the event-selection criteria, all single-detector hits with recoil energies in the range 1.6–10 keV<sub>nr</sub> and ionization energy consistent with nuclear recoils were removed from the sample, i.e. blinded. An exception was made for periods following  $^{252}\text{Cf}$  calibrations, when background rates were higher because of neutron activation of the detectors and their copper housings. This “open” dataset constitutes 97 kg-days of exposure that is distinct from the 577 kg-days of data analyzed for WIMPs, and was not used in the final limit calculation or to optimize selection criteria.

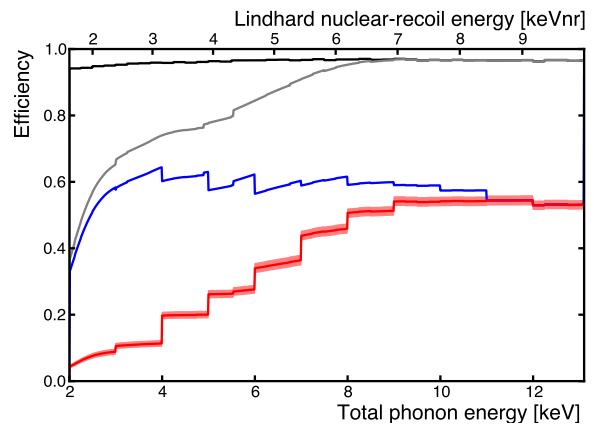


FIG. 1. Cumulative efficiencies after sequential application of each stage of event selection. From top to bottom, these are data-quality criteria, trigger and analysis threshold efficiencies, preselection criteria, and BDT discrimination with 68% C.L. (stat. + syst.) uncertainty band. Steps are due to the combination of smooth fits of the trigger efficiency and binned measurements. For illustrative purposes, an approximate nuclear-recoil energy scale is provided.

For the detectors analyzed, the standard deviation of the baseline noise is  $\lesssim 260$  eV for summed phonon channels and  $\lesssim 460$  eV<sub>ee</sub> (electron-recoil equivalent) for individual ionization channels. The electron- and nuclear-recoil energy scales are calibrated in a fashion similar to the CDMS II light-WIMP search [17] using  $^{133}\text{Ba}$  and  $^{252}\text{Cf}$  sources respectively. A small ( $\lesssim 10\%$ ) variation of the phonon signal gain with the cryostat base temperature, which varied over the range 54–62 mK, is taken into account by the phonon calibration. In each detector, the mean ionization energy of nuclear recoils as a function of total phonon energy, as determined from  $^{252}\text{Cf}$  calibration data, is consistent with, or slightly below, the prediction of Lindhard [24, 25]. A nuclear-recoil band was constructed by accepting events within  $3\sigma$  of the mean ionization energy. Nuclear-recoil equivalent energies are reconstructed from the total phonon energy by subtracting the contribution of Luke-Neganov phonons [26, 27] corresponding to the mean nuclear-recoil ionization response for the respective total phonon energy.

Hardware trigger thresholds for each detector were adjusted several times during the WIMP search. For each period of constant trigger threshold, the trigger efficiencies as functions of total phonon energy were measured using  $^{133}\text{Ba}$  calibration data. The fit results were found to be consistent with, but less precise than ones obtained using  $^{252}\text{Cf}$  and multiple-hit WIMP-search data. Analysis thresholds are set to be  $1\sigma$  below the energy at which the detector trigger efficiency is 50%. For some time intervals, analysis thresholds are raised further according to baseline noise levels. The combined efficiency is an exposure-weighted sum of the measured efficiency for

each detector and period, shown in Fig. 1.

To be selected as WIMP candidates, triggered events had to pass three levels of data-selection criteria: data quality, preselection, and event discrimination. Figure 1 shows the cumulative efficiency after applying each level of selection criteria and the analysis thresholds. The first level of criteria (data quality) rejects poorly reconstructed and noise-induced events. Periods of abnormal noise are removed by requiring that the pre-trigger baseline noise of each event be consistent with normal periods. Spurious triggers caused by electronic glitches and low-frequency noise in the phonon channels, which populate the low-energy region, were rejected using a pulse-shape discrimination method. Using a Monte Carlo pulse simulation that added experimental noise to template pulses to account for variation in the noise environment, the WIMP acceptance of this data-quality selection was determined to be  $\gtrsim 95\%$ .

The second level of event-selection criteria (preselection) removes event configurations inconsistent with WIMPs. Events coincident with the muon veto are rejected (98.7% acceptance). A single-scatter requirement removes events with energy depositions in multiple detectors, a common signature for background interactions but not expected for a WIMP-nucleon scatter ( $>99\%$  acceptance, with losses due to noise fluctuations). We also require events to lie within the  $3\sigma$  nuclear-recoil band and have phonon partitions consistent with bulk nuclear recoils. A loose fiducial volume constructed from the ionization partitions further restricts events to be consistent with bulk nuclear recoils. In the radial direction, events near the detectors' sidewalls are rejected by requiring the guard electrodes on both faces to be within  $2\sigma$  from the mean of the baseline noise. For one detector (T5Z3) that has a malfunctioning guard electrode on one side, this requirement is applied on only the functioning face. A second detector (T5Z2) suffered sporadic excess noise on one guard, so only the guard on the functioning face was used for part of the dataset. In the  $z$  direction, events on the flat faces are excluded by requiring that the inner electrodes on each side measure similar ionization energies [23].

The final level of event selection (discrimination) uses a boosted decision tree (BDT) [28]. The discriminators used by the BDT are the total phonon energy, ionization energy, phonon radial partition and phonon  $z$  partition. Near threshold, the latter two variables provide identification of surface events superior to the ionization partitions, while the two energy quantities together optimize the discrimination at low energy where the electron- and nuclear-recoil bands overlap. A BDT was trained for each detector using simulated background events (described below) and nuclear recoils from  $^{252}\text{Cf}$  calibration weighted to mimic a WIMP energy spectrum, accounting for the selection criteria acceptance. The BDT thresholds for individual detectors were chosen simultaneously to

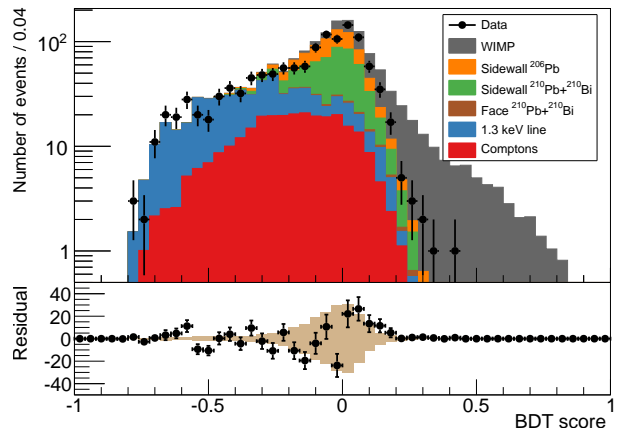


FIG. 2. Top: Stacked histogram showing the components of the background model passing the preselection criteria, summed over all detectors. For comparison, a  $10 \text{ GeV}/c^2$  WIMP with cross section  $6 \times 10^{-42} \text{ cm}^2$  is shown on top of the total background. Events passing preselection criteria are overlaid (markers with statistical errors). A  $p$ -value statistic comparing the data to model prediction is 14% for this selection. Bottom: Difference between the data and the background expectation. Tan bars indicate the systematic uncertainty (68% C.L.) on the background estimate. The background spectrum was computed prior to unblinding and was not fit or rescaled to match the data.

optimize the expected 90% confidence level (C.L.) Poisson upper limit of the rate of passing events per WIMP exposure. The BDT was trained and optimized separately for 5, 7, 10 and 15  $\text{GeV}/c^2$  WIMPs. Candidate events that pass any of the four WIMP-mass optimizations are accepted into the signal region. When a limit is set using the optimum interval method [29, 30], this acceptance technique provides sensitivity to a range of masses, but incurs only modest sensitivity loss compared to an analysis optimized at every WIMP mass. In addition to the BDT, two other discrimination methods were developed and similarly optimized for WIMP masses between 5 and 15  $\text{GeV}/c^2$ . The BDT was chosen as the primary discrimination method before unblinding because of its better expected sensitivity on the background simulation data.

The acceptance of the preselection criteria and the BDT was evaluated using the fraction of  $^{252}\text{Cf}$  nuclear recoils passing as a function of energy. Unlike WIMPs, the  $^{252}\text{Cf}$  neutrons can multiply scatter within a single detector, which necessitates correcting the acceptance upwards by  $\sim 25\%$  above  $\sim 5 \text{ keV}_{\text{nr}}$  based on a Geant4 [31] neutron simulation, including constraints on the resolution effects and the size of the fiducial volume. The uncertainty of the total acceptance is dominated by systematic uncertainty on the size of the fiducial volume and is shown in Fig. 1.

A background model was developed that includes

Compton recoils from the gamma-ray background; 1.1–1.3 keV X-rays and Auger electrons from L-shell electron-capture (EC) decay of  $^{65}\text{Zn}$ ,  $^{68}\text{Ga}$ ,  $^{68}\text{Ge}$  and  $^{71}\text{Ge}$ ; and decay products from  $^{210}\text{Pb}$  contamination on the detectors and their copper housings. We normalize the flat Compton background to the observed rate of electron recoils in the range 2.6–5.1 keV<sub>ee</sub>. The average rate of L-shell EC events is estimated by scaling the observed rate in the open dataset by the ratio of the K-shell event rates in the WIMP-search and open datasets. We use Geant4 to simulate the implantation and decay of  $^{222}\text{Rn}$  daughters starting from  $^{214}\text{Po}$  as described in [23]. Background components from  $^{210}\text{Pb}$  decay products (betas, conversion electrons, X-rays),  $^{210}\text{Bi}$  betas, and  $^{206}\text{Pb}$  nuclei from  $^{210}\text{Po}$  decays are considered, with rates normalized to the alpha and  $^{206}\text{Pb}$  decay products of  $^{210}\text{Po}$  under the assumption of secular equilibrium.

The background model is implemented using events from high-energy sidebands and calibration data as templates for low-energy backgrounds. Ionization and phonon pulses are scaled to lower energies, injected with noise from randomly triggered events throughout the data, and reconstructed as actual data. The simulation is then weighted to match the background energy spectra.  $^{133}\text{Ba}$  calibration data and K-shell EC events are used as templates for the Compton recoils and L-shell EC events, respectively. Templates for  $^{210}\text{Pb}$  daughters are sampled from high-energy betas and  $^{206}\text{Pb}$  recoils.

The background model was finalized prior to unblinding and predicted  $6.1^{+1.1}_{-0.8}$  (stat.+syst.) events. Simulations of radiogenic and cosmogenic neutrons, as described in [21], predict an additional  $0.098 \pm 0.015$  (stat.) events. Figure 2 shows the individual components of the background model as a function of the 10 GeV/ $c^2$  BDT discrimination parameter after applying the preselection criteria. These estimates included only known systematic effects, which were not certain to be exhaustive before unblinding. Because the accuracy of background modeling required for a full likelihood analysis is difficult to achieve in a blind analysis of this type, the decision was made before unblinding to report an upper limit on the WIMP-nucleon cross section.

Upon unblinding, eleven candidates were observed as indicated in Fig. 3. The events were found to be of high quality and occurring during good periods of experimental operation, except for the lowest-energy candidate, which has an abnormal pulse shape and is suspected to be noise. As seen in Table I, the observed number of events is consistent with the background prediction for most detectors. However, the three high-energy events in detector T5Z3 strongly disagree with the background prediction. The probability to observe at least this many background events is  $4 \times 10^{-4}$ . These events are observed on the only detector in this dataset that has one ionization guard electrode shorted to ground. Although the background model attempts to account for the shorted

channel, we suspect that the altered electric field resulted in a selection of background model templates for this detector that was not representative of the true background.

The background model is compared to unblinded events passing all preselection criteria in Fig. 2. The systematic uncertainty, shown with tan fill, is dominated by the uncertainty of the expected ionization of sidewall events originating from  $^{210}\text{Pb}$  and  $^{210}\text{Bi}$ . P-value statistics comparing the data passing the preselection criteria with the blind background model prediction, summed over the bins of BDT score, range from 8–26% for the BDTs trained to each of the four masses. This reasonable compatibility suggests that the background model correctly reproduces most features of the true background when summed over all detectors.

A 90% C.L. upper limit on the spin-independent WIMP-nucleon cross section was calculated using the optimum interval method without background subtraction. The calculation used standard halo assumptions as discussed in [32]. The result is shown in Fig. 4. Statistical and systematic uncertainties in the fiducial-volume efficiency, the nuclear-recoil energy scale, and the trigger efficiency were propagated into the limit by Monte Carlo and are represented by the narrow gray band around the limit. All uncertainties are uncorrelated across detectors except the systematic uncertainty of the fiducial-volume efficiency. The limit is consistent with the expected sensitivity for masses below 10 GeV/ $c^2$  as shown by the green band in Fig. 4. The discrepancy above 10 GeV/ $c^2$  is due to the three high-energy events in T5Z3, which are in tension with the background expectation.

This work represents the first search for WIMPs with the background rejection capability of SuperCDMS detectors. A physically motivated background model gen-

| Detector | Candidate energies [keV <sub>nr</sub> ] | Expected background    |
|----------|---|------------------------|
| T1Z1     | —                                       | $0.03^{+0.01}_{-0.01}$ |
| T2Z1     | 1.7, 1.8                                | $1.4^{+0.2}_{-0.2}$    |
| T2Z2     | 1.9, 2.7                                | $1.8^{+0.4}_{-0.3}$    |
| T4Z2     | —                                       | $0.04^{+0.02}_{-0.02}$ |
| T4Z3     | —                                       | $1.7^{+0.4}_{-0.3}$    |
| T5Z2     | 5.8, 1.9, 3.0, 2.3                      | $1.1^{+0.3}_{-0.3}$    |
| T5Z3     | 7.8, 9.4, 7.0                           | $0.13^{+0.06}_{-0.04}$ |

TABLE I. Energies of candidate events in each detector, labeled by tower (first number) and position within tower from top to bottom (second number). Expected background is based on the model used to train the BDT and includes the estimated systematic uncertainty. Differences in expected background across detectors reflect different trigger thresholds and background event rates. Event energies are calculated using the measured mean ionization energy for nuclear recoils.



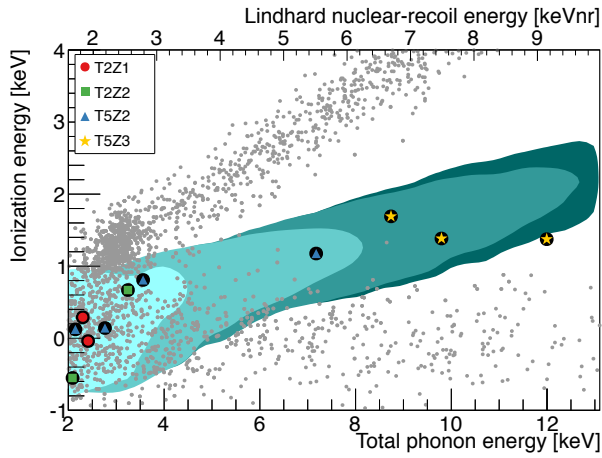


FIG. 3. Small gray dots are all veto-anticoincident single-scatter events within the ionization-partition fiducial volume that pass the data-quality selection criteria. Large encircled shapes are the 11 candidate events. Overlapping shaded regions (from light to dark) are the 95% confidence contours expected for 5, 7, 10 and 15  $\text{GeV}/c^2$  WIMPs, after application of all selection criteria. The three highest-energy events occur on detector T5Z3, which has a shorted ionization guard. Above the expected signal contours is a band of events corresponding to bulk electron recoils, including the 1.3 keV activation line at a total phonon energy of  $\sim 3$  keV. High-radius events near the detector sidewalls form the wide band of events with near-zero ionization energy. For illustrative purposes, an approximate nuclear-recoil energy scale is provided.

erally agrees with the data, except for the detector with a shorted ionization guard. This analysis strongly disfavors a WIMP-nucleon scattering interpretation of the excess reported by CoGeNT, which also uses a germanium target. Similar tension exists with WIMP interpretations of several other experiments, including CDMS II (Si), assuming spin-independent interactions and a standard halo model. New regions of WIMP-nucleon scattering for WIMP masses below  $6 \text{ GeV}/c^2$  are excluded.

The SuperCDMS collaboration gratefully acknowledges the contributions of numerous engineers and technicians. In addition, we gratefully acknowledge assistance from the staff of the Soudan Underground Laboratory and the Minnesota Department of Natural Resources. The iZIP detectors were fabricated in the Stanford Nanofabrication Facility, which is a member of the National Nanofabrication Infrastructure Network. This work is supported in part by the National Science Foundation, by the United States Department of Energy, by NSERC Canada, and by MultiDark (Spanish MINECO). Fermilab is operated by the Fermi Research Alliance, LLC under Contract No. De-AC02-07CH11359. SLAC is operated under Contract No. DE-AC02-76SF00515 with the United States Department of Energy.

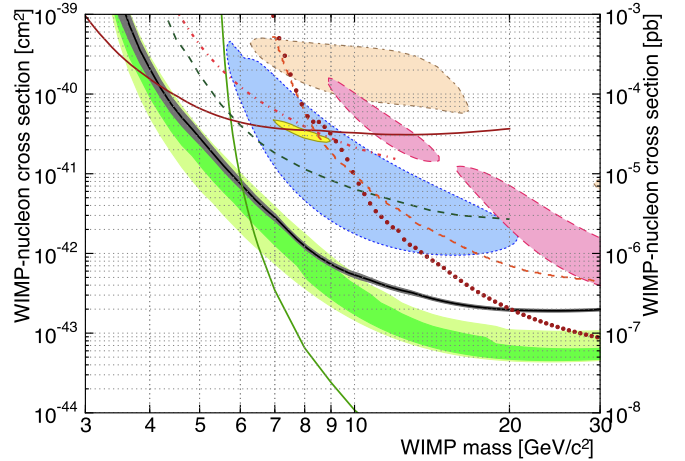


FIG. 4. The 90% confidence upper limit (solid black) based on all observed events is shown with 95% C.L. systematic uncertainty band (gray). The pre-unblinding expected sensitivity in the absence of a signal is shown as 68% (dark green) and 95% (light green) C.L. bands. The disagreement between the limit and sensitivity at high WIMP mass is due to the events in T5Z3. Closed contours shown are CDMS II Si [3] (dotted blue, 90% C.L.), CoGeNT [4] (yellow, 90% C.L.), CRESST-II [5] (dashed pink, 95% C.L.), and DAMA/LIBRA [33] (dash-dotted tan, 90% C.L.). 90% CL exclusion limits shown are CDMS II Ge [21] (dotted dark red), CDMS II Ge low-threshold [17] (dashed-dotted red), CDMSlite [34] (solid dark red), LUX [35] (solid green), XENON10 S2-only [19, 36] (dashed dark green), and EDELWEISS low-threshold [18] (dashed orange).

\* Corresponding author: [adama@mit.edu](mailto:adama@mit.edu)

- [1] J. L. Feng, *Ann. Rev. Astro. Astrophys.*, **48**, 495 (2010).
- [2] M. W. Goodman and E. Witten, *Phys. Rev. D*, **31**, 3059 (1985).
- [3] R. Agnese *et al.* (CDMS Collaboration), *Phys. Rev. Lett.*, **111**, 251301 (2013).
- [4] C. E. Aalseth *et al.* (CoGeNT Collaboration), *Phys. Rev. D*, **88**, 012002 (2013).
- [5] G. Angloher *et al.*, *Eur. Phys. J. C*, **72**, 1971 (2012).
- [6] R. Bernabei *et al.*, *Eur. Phys. J. C*, **67**, 39 (2010).
- [7] D. Hooper and T. Linden, *Phys. Rev. D*, **84**, 123005 (2011).
- [8] D. B. Kaplan, *Phys. Rev. Lett.*, **68**, 741 (1992).
- [9] D. E. Kaplan, M. A. Luty, and K. M. Zurek, *Phys. Rev. D*, **79**, 115016 (2009).
- [10] A. Falkowski, J. Ruderman, and T. Volansky, *J. High Energy Phys.*, **1105**, 106 (2011).
- [11] R. R. Volkas and K. Petraki, *Int. J. Mod. Phys. A*, **28**, 1330028 (2013).
- [12] K. M. Zurek, (2013), [arXiv:1308.0338](https://arxiv.org/abs/1308.0338).
- [13] R. Essig, J. Kaplan, P. Schuster, and N. Toro, Submitted to *Physical Review D* (2010), [arXiv:1004.0691](https://arxiv.org/abs/1004.0691).
- [14] C. Cheung, J. T. Ruderman, L.-T. Wang, and I. Yavin, *Phys. Rev. D*, **80**, 035008 (2009).
- [15] D. Hooper and W. Xue, *Phys. Rev. Lett.*, **110**, 041302 (2013).

- (2013).
- [16] D. S. Akerib *et al.* (CDMS Collaboration), Phys. Rev. D, **82**, 122004 (2010).
  - [17] Z. Ahmed *et al.* (CDMS Collaboration), Phys. Rev. Lett., **106**, 131302 (2011).
  - [18] E. Armengaud *et al.* (EDELWEISS Collaboration), Phys. Rev. D, **86**, 051701 (2012).
  - [19] J. Angle *et al.* (XENON10 Collaboration), Phys. Rev. Lett., **107**, 051301 (2011).
  - [20] J. Sander *et al.*, AIP Conf. Proc., **1534**, 129 (2012).
  - [21] Z. Ahmed *et al.* (CDMS Collaboration), Science, **327**, 1619 (2010).
  - [22] D. Akerib *et al.* (CDMS Collaboration), Phys. Rev. D, **72**, 052009 (2005).
  - [23] R. Agnese *et al.* (SuperCDMS Collaboration), Appl. Phys. Lett., **103**, 164105 (2013).
  - [24] J. Lindhard, V. Nielsen, M. Scharff, and P. Thomsen, *Integral Equations Governing Radiation Effects* (Munksgaard i komm., Copenhagen, Denmark, 1963).
  - [25] J. Lewin and P. Smith, Astropart. Phys., **6**, 87 (1996).
  - [26] B. Neganov and V. Trofimov, Otkrytie. Izobreteniya, **146**, 215 (1985).
  - [27] P. Luke, J. Appl. Phys., **64**, 6858 (1988).
  - [28] A. Hoecker *et al.*, PoS ACAT, 040 (2007), [arXiv:physics/0703039](https://arxiv.org/abs/physics/0703039).
  - [29] S. Yellin, Phys. Rev. D, **66**, 032005 (2002).
  - [30] S. Yellin, (2007), [arXiv:0709.2701](https://arxiv.org/abs/0709.2701).
  - [31] S. Agostinelli *et al.* (Geant4), Nucl. Instrum. Methods A, **506**, 250 (2003).
  - [32] Z. Ahmed *et al.* (CDMS Collaboration), Phys. Rev. D, **83**, 112002 (2011).
  - [33] C. Savage, G. Gelmini, P. Gondolo, and K. Freese, JCAP, **0904**, 010 (2009).
  - [34] R. Agnese *et al.* (SuperCDMS Collaboration), Phys. Rev. Lett., **112**, 041302 (2014).
  - [35] D. S. Akerib *et al.*, Accepted to Physical Review Letters (2013), [arXiv:1310.8214](https://arxiv.org/abs/1310.8214).
  - [36] J. Angle *et al.* (XENON10 Collaboration), Phys. Rev. Lett., **110**, 249901(E) (2013).